Available online at www.sciencedirect.com
SCIENCE DIRECT
International Journal of Heat and Fluid Flow 27 (2006) 502–513
International Journal of HEAT AND FLUID FLOW
www.elsevier.com/locate/ijhff

# Effect of swirl on pure turbulent thermal plume development

Minh Vuong Pham, Frédéric Plourde *, Son Doan Kim

*LET—ENSMA, UMR CNRS 6608, Laboratoire D'Etudes Thermiques, 1 Avenue Clément Ader, BP 40109, 86960 Chasseneuil Futuroscope Cedex, France*

Received 13 June 2005; received in revised form 25 November 2005; accepted 10 December 2005
Available online 2 February 2006

**Abstract**

Pure thermal plumes have been experimentally investigated under swirling conditions. Such conditions are applied upon the heated source impinging directly on the plume development. Results clearly underlined the existence of a threshold swirling number. Below the latter, i.e., at small swirling velocities, ascendant flow behaves like a classical static plume while at a high swirling number, the flow is clearly affected even if characteristic power laws are still valid. However, swirling of the source favors transition from laminar to turbulence as well as breakdown of coherent structures all around the plume motion. A direct measurement method was applied in order to assess instantaneous entrainment coefficients, and results clearly show appreciable influence of the swirling motion on the plume development. The driving mechanisms, i.e., contraction and expulsion phenomena, are strongly amplified and as a consequence directly interact on entrainment.


*Keywords:* Plume; Buoyancy; Turbulence; Swirl

## 1. Introduction

A pure thermal plume, i.e., without any momentum mass injection, is a very complex flow despite its relatively simple geometry. Such complexity is mainly due to the development of strong interactions between inertial and buoyancy forces leading to abrupt transition from laminar to turbulence. Turbulence in unbounded flows is well-documented in the literature both for a plume originating from a point source and for a plane plume arising from a line source. In such configurations, Bill and Gebhart (1975) pointed out that a flow subject to naturally occurring disturbances is found to selectively amplify disturbance below a given cut-off frequency. Turbulence is actually an event subsequent to the initial instability of a laminar flow, and perturbations may grow in amplitude. Bastiaans et al. (2000) conducted direct simulations in a confined area emphasizing symmetry bifurcation and results underline that in such configurations, transition is mainly driven by mechanisms such as Hopf and Pitchfork bifurcation at low heat input. Aside from transition, one may also find a wide range of articles dedicated to the characterization of buoyant flows even though studies dedicated to pure thermal plumes are less numerous. In addition, numerical as well as experimental results often refer to analytical development; the latter, initially developed by Taylor (1945), entails that a turbulent buoyancy element expands at the expense of the quiescent surrounding fluid through entrainment of exterior fluid. Morton et al. (1956) proposed similarity solutions in both uniform and stratified environments while Turner (1969) extended the analysis to plumes arising from source of buoyancy and showed that these flows can be related to equivalent point sources of buoyancy only. Recently, Agrawal and Prasad (2004) implemented integral methods to derive similarity solutions for several quantities of interest such as turbulent kinetic energy production term for instance. According to their findings, and contrarily to conventional belief, entrainment velocity was not found to be proportional to ascendant

* Corresponding author.
*E-mail address:* frederic.plourde@let.ensma.fr (F. Plourde).

0142-727X/$ - see front matter © 2006 Elsevier Inc. All rights reserved.
doi:10.1016/j.ijheatfluidflow.2005.12.001

**Nomenclature**

$D$ heating source diameter (m)
$g$ gravity acceleration in the $z$ axial direction ($ms^{-2}$)
$Gr_L = gL_Z^3 \frac{\Delta T_s}{T_\infty} \frac{\rho_\infty^2}{\mu_\infty^2}$ Grashof number
$I_u = \frac{\sqrt{\overline{u_r'^2}+\overline{u_\theta'^2}+\overline{u_z'^2}}}{\bar{u}_{z,c}}$ dynamic turbulent intensity
$I_t = \frac{\sqrt{\overline{\Theta'^2}}}{\Theta_c}$ thermal turbulent intensity
$L_X \times L_Y \times L_Z$ dimension of the enclosure (m)
$\dot{m}$ non-dimensional plume mass flow rate
$\dot{m}_e$ non-dimensional entrained mass flow
$N$ rotation frequency of the heated source (Hz)
$r$, $z$ radial and axial co-ordinates scaled by $D$
$R_0 = \frac{\pi DN}{U_{ref}}$ swirling number
$T$ temperature (°C)
$\Delta T_s = T_s - T_\infty$ characteristic temperature difference (°C)
$U_{ref} = \sqrt{gD\frac{\Delta T_s}{T_\infty}}$ characteristic reference velocity (m/s)
$u_x$, $u_y$, $u_z$ Cartesian velocity components normalized by $U_{ref}$
$u_r$, $u_\theta$, $u_z$ cylindrical velocity components transformed from $u_x$, $u_y$, $u_z$
$x$, $y$, $z$ non-dimensional Cartesian co-ordinate normalized by $D$
$\lambda$ normalized plume radius
$\alpha$ instantaneous entrainment coefficient
$\bar{\alpha}$ mean entrainment coefficient
$\beta$ plume expansion angle (°)
$\theta_0$ angle between view of camera and normal of measurement plane (°)
$\Theta = \frac{T-T_\infty}{T_s-T_\infty}$ normalized temperature
$\rho$ fluid density normalized by $\rho_\infty$
$\mu$ dynamic viscosity (kg/m/s)

*Subscripts*
c geometrical axis location
s heating source
$\infty$ referred to quiescent environment
max maximum level

velocity in an axisymmetric plume. Although this finding seems to be in contradiction with most of the experimental results dedicated to pure thermal plumes (Dehmani et al., 1996a; Shabbir and George, 1994; Agator and Doan Kim, 1982), it is true that conducting experimental investigations to assess entrainment is a rather difficult task. To better analyse entrainment in pure thermal plume, it is important to take into account the contribution of the $\overline{\rho' u'}$ density–velocity (Dibble et al., 1987), which is classically overlooked. To avoid this type of assumption, a direct measurement technique is required such as that of Ricou and Spalding (1961), who tried in the early sixties to measure entrained mass flow rate by surrounding jets with a cylindrical porous plate. While this mode of investigation was by no means accurate, such a concept introduced an excellent idea that may nowadays be adapted more efficaciously to pure thermal plume. Thus, Pham et al. (2005) recently experimentally investigated a pure thermal plume, and the particle imaging velocimetry technique was used to fully depict flow field inside and outside the plume. A new direct method never previously applied to plumes allows one to estimate entrainment provided by the plume when measuring velocity entering into the plume. In addition, entrainment was described with time, and time-dependent analysis exhibited contraction and expulsion phases characterising ascendant motion development. The latter is mainly driven by turbulent structure behaviour and such phases act literally on engulfment. In any event, these new experimental results confirm those of Basu and Narasimha (1999), who numerically simulated behaviour in a non-heated and a heated jet. They put forward the hypothesis that enhancement of vorticity due to vortex stretching favours intense structures that tend to attract fluid from the quiescent environment. Even if the pure thermal plume has been extensively studied in the literature, whether it be plume arising from axisymmetric or from line sources, evolving in either a stratified or a non-stratified environment, these new findings allow the observer to somewhat enhance his knowledge of such flows. As regards the pursuit of the same objective, pure thermal plume feature under swirling conditions of its heated source has never, as far as we know, been investigated. Consequently, conclusive investigation is the main goal of the present study. It is important to underline that several other studies (Helfrich, 1994; Ayotte and Fernando, 1994; Julien et al., 1999), mainly numerical investigations, have been performed in order to analyse plume feature developing in a rotating environment; their results suggest that expansion of plume through entrainment may be suppressed under strong rotating conditions. In such cases, the Coriolis force dominates plume inertial force. Our objectives are somewhat different; while its heated source is being rotated, thermal plume is experimentally investigated. The first part is dedicated to experimental set-up and measurement techniques used to assess flow field behaviour under swirling conditions. Experiments were conducted under a wide range of rotation frequencies of the source on a turbulent plume with a Grashof number of $Gr_{L_z} = 9.0 \times 10^{10}$ and for each case an equivalent $S$ swirling number is estimated. Mean and turbulent statistics are then presented under swirling conditions; the results mainly address the way in which rotation of the source more or less altered the classical

well-known laws issued from a static thermal plume arising in a quiescent environment. Transition from laminar to turbulence is also carefully analyzed. Finally, the direct method has been applied in order to depict influence of the swirling motion on entrainment mechanisms.

## 2. Experimental set-up and measurement techniques

A schematic view of the experimental set-up is shown in Fig. 1. The heating source is made up of a metallic disk with a $D$ diameter of 0.1 m and a thickness of 0.02 m. The heat is provided by a heating resistance wire which is located directly inside the metallic disk. A regulated AC of 1 kV A supplied electric power and was able to keep the disk temperature at a constant level of $T_s = 400$ °C. A pin is assembled to the disk centered on the geometrical axis and the pin is linked to a stepper motor by a driving belt. The rotation speed is controlled by means of magnetic detector recording in time the rotation frequency of the disk. The latter varied within a range of 0.0–10 Hz and accuracy of the rotating system was found to be less than 5% of the rotating velocity. Each experimental test case is referred to an additional parameter, the swirling number $S$. Table 1 lists the corresponding $S$ levels to the $N$ rotating frequency. The disk was located in a large enclosure of $2\text{ m} \times 2\text{ m} \times 2.5\text{ m}$ filled with air and the disk was not flush-mounted, but a height of 0.01 m was introduced between the disk and the enclosure floor in order to stabilize plume development (Guillou and Doan Kim, 1983). The enclosure in which the plume developed was located in a larger room of $6\text{ m} \times 6\text{ m} \times 6\text{ m}$ which was equipped with an air-conditioning system and its temperature was kept at a constant level of 20 °C. Thus, stratification of air temperature outside ascendant motion was reduced as low as possible during experiments, and this gradient was regularly controlled by measuring plume outside temperature with Al–Cr thermocouple of 12.7 μm diameter. The highest temperature gradient during experiments was found to be equal to 0.4 °C/m and such stratification level may be considered as negligible with regard to any thermal stratification influence (Dehmani et al., 1996b). In accordance with the whole temperature acquisition system, fluid temperature measurement errors were found to be less than 0.01 °C. The thermocouple was fixed on a 3D traverse system allowing the latter to determine height-wise temperature profile. The traverse system resolution is equal to $10^{-4}$ m.

In order to measure the flow field velocity, particle imaging velocimetry technique (PIV) was employed and we performed 2D as well as 3D stereoscopic PIV measurements. For both of these measurements, $1024 \times 1280$ pixel Hamamatsu Hisence cameras were used. Each pixel sized $6.7 \times 6.7$ μm and a pair of images was recorded at a 9.0 Hz rate. To illuminate the flow field, a 50 mJ frequency doubled Nd–Yag laser was set-up in synchronization with cameras. The laser plane was orientated in accordance with the types of measurements employed. 2D measurements were performed with a $x$–$z$ laser plane integrating the geometrical axis while stereoscopic measurements were carried out with a $x$–$y$ laser plane at $z$ several heights (Fig. 2). In the 2D configuration, only one camera was necessary and it was equipped with a 28 mm lens focusing a plane at a 1.0 m interval. The plane of measurement was then approximately 26 cm × 30 cm. The time delay between two consecutive pictures was arbitrarily fixed and varied from $2 \times 10^{-3}$ s up to $20 \times 10^{-3}$ s and the interrogation zone

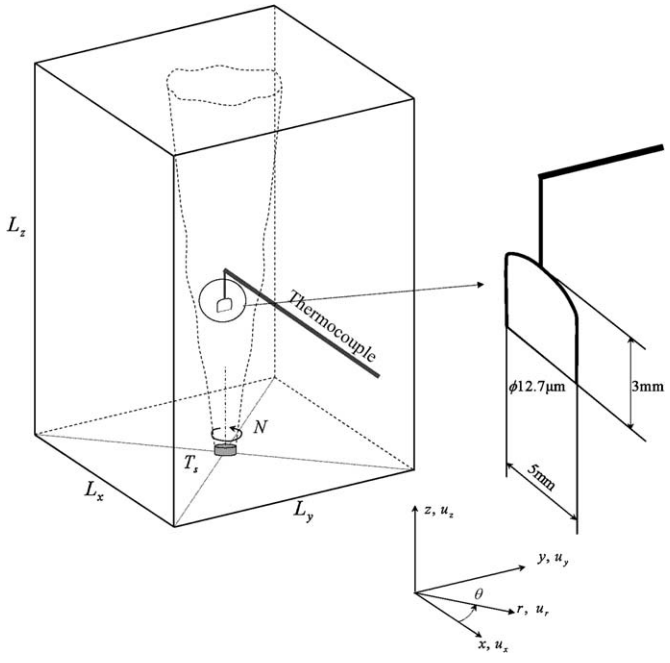


Fig. 1. Schematic of the thermal rotating plume experiment.

Table 1
Corresponding rotation frequency and $S$ swirling number

| $N$ (Hz) | 0 | 0.5 | 1.0 | 1.5 |
|---|---|---|---|---|
| $R_0$ | 0.0 | 0.14 | 0.27 | 0.41 |

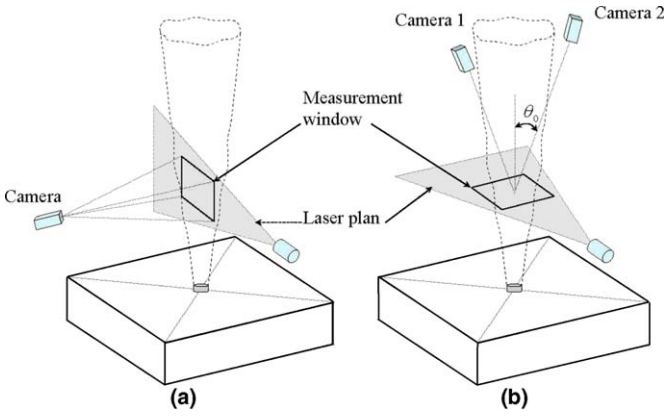


Fig. 2. Measurement set-up using (a) classical 2D PIV technique and (b) stereoscopic PIV technique.

was set to $32 \times 32$ pixels using 50% overlapping, which corresponds to a $63 \times 79$ vector resolution in the $x$–$z$ plane.

In the case of stereoscopic PIV measurements, two cameras were located at 1 m from the laser plane so as to obtain 26 cm × 30 cm of window measurement. Each camera was positioned at a 30° angle from the normal measurement plane in order to obtain stereo views of the plane in accordance with the laser sheet orientation (Alkislar et al., 2000). Calibration procedures allow the observer to avoid any perspective distortion arising from the skewed orientation of the cameras. After processing images from each camera, data also had to be processed so as to evaluate the third velocity component perpendicular to the laser sheet plane. At each plane studied, over 200 s were necessary in order to acquire 800 instantaneous velocity fields at a rate of 4.0 Hz.

Accuracy of velocity measurements through PIV method was estimated. All our measurements were performed by using glycerin particles originating from a smoke generator and it is assumed that the diameter particle ranged from 5 to 10 μm. According to the diameter, density and velocity level of the flow, one can likewise assume that the bias due to dynamic-particles is around 0.2%. To estimate processing errors, a picture was taken as a reference while a second one was created by introducing a previously known displacement throughout the complete first one. After that, it may be necessary to compare the PIV estimation with regard to the introduced displacement. The processing errors are mainly linked to the algorithm and may be estimated as 0.1 pixels that correspond to 1.8% error for a standard $32 \times 32$ interrogation window size cross-correlation. The beam steering error is linked to the index of refraction change due to density variation in thermal plume but along with image distortion effects, such error may be considered as negligible (Muñiz, 2000).

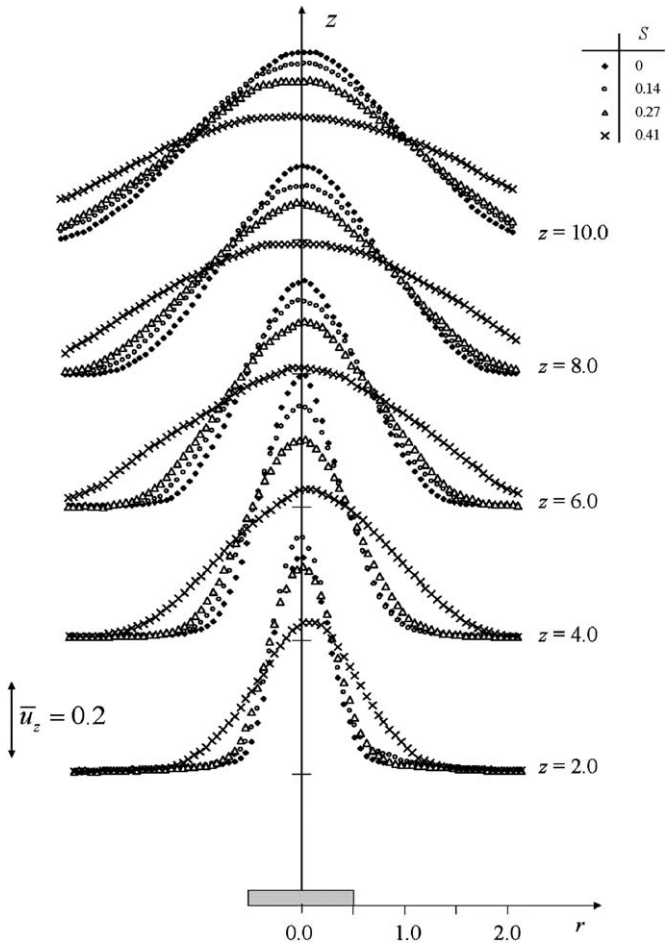


Fig. 3. Radial profiles of the $\bar{u}_z$ mean axial velocity component change with regard to $z$ and parametrised by $S$.

## 3. Results and discussion

### 3.1. Thermal plume behaviour

As underlined in Section 1, thermal plumes have been extensively studied in the past but to our knowledge the effect of source rotation on thermal plume behaviour has never been investigated. One should nonetheless mention research developed by Elsner and Kurzak (1989), who formulated a semi-preserving concept on a free non-isothermal swirling jet. However, even though attention had been paid to the temperature field and turbulent heat diffusion, buoyancy was not taken into account due to jet velocities involved. In order to investigate the role of source rotation on plume behaviour, the first step consists in studying the mean velocity field in a pure thermal plume for a wide range of rotation frequencies of the heated source. Fig. 3 presents the $\bar{u}_z$ mean longitudinal profiles with regard to the $r$ radial location at several $z$ heights and for four rotating frequencies ranging from $0 \leqslant N \leqslant 1.5$ Hz. Before giving detailed analysis of the measurements obtained under swirling conditions, it is necessary to emphasize that results arising from the same experimental set-up but under non-swirling conditions ($N = 0$ Hz) have recently been published (Pham et al., 2005). On the basis of 2D and stereoscopic 3D PIV measurements, it was shown that flow field behaves like a pure thermal plume, i.e., specific attention was given to experimental conditions in order to ensure that no thermal stratification would occur during experiments. Thus, according to this observation, one can consider the plume development as taking place in an infinite open space. As shown in Fig. 3 under non-swirling conditions, velocity profiles present a sharp maximum peak at $r = 0$ in the vicinity of the heated source ($z = 2.0$). Such a shape is generally observed in that area, and it corresponds to fluid contraction due to severe interactions between the ascendant flow development and entrainment of fluid surrounding the former. However, a contradictory trend rapidly develops and the higher $z$ the wider the profile.

Under swirling conditions, the amplitude of the maximum reached at $r = 0$ is directly linked to rotation frequency. From a static case to $N = 0.5$ Hz, i.e., $S = 0.14$, a slight increase occurs, yet increase of $N$ produces a completely different trend on the maximum, which decreases significantly. Concerning the profile shape of the vertical

velocity component, all the profiles come close to fitting a single distribution except for the highest swirling frequency studied, i.e., $N = 1.5$ Hz ($S = 0.41$). Actually, such swirling condition enhances lateral expansion of the profile and a 40% decrease is observed in the maximum velocity amplitude between the static case ($S = 0$) and the highest frequency studied ($S = 0.41$). When studying profiles at higher positions ($z \geqslant 2.0$), swirling condition emphasizes the lateral expansion of the ascendant flow and alters the amplitude reached. The higher the frequency $N$, i.e., the higher the swirling number $S$, the smaller the amplitude and the wider the profiles. To analyse more accurately how swirl motion affects the ascendant fluid motion, the change of the characteristic radius $\lambda$ of the plume has been studied with regard to $z$ and in conjunction with the magnitude of the swirling number $S$. Following Turner's definition, $\lambda$ is obtained by integrating radial profile of the vertical velocity component along a given section. Then, under static conditions, the change of $\lambda$ is linear with regard to $z$ in the auto-similar region, i.e., in the fully turbulent region. As shown in Fig. 4, the linear change of $\lambda$ with regard to $z$ occurs for $z$ beyond 3.5 approximately in the non-swirling condition. However, as already observed following lateral $\bar{u}_z$ velocity profiles, swirl motion of the heated source greatly affects the characteristic size of the plume. As soon as rotation arises, even at a low frequency, lateral expansion of the ascendant flow is favoured. For instance, at $S = 0.14$ ($N = 0.5$ Hz), the plume width becomes larger than the one obtained in the non-swirling case but this does not affect its linear dependency to $z$; the slope is simply higher for $S = 0.14$ than for $S = 0$. Such a trend is amplified with the increase of $S$. In the highest frequency shown ($S = 0.41$), the linear change with regard to $z$ already occurs at $z = 2.0$. To highlight how plume width is linked to source rotation frequency, Fig. 5 reveals the variation of $\lambda$ with regard to $S$ at two different heights, and it is interesting to underline that at both vertical locations shown, $\lambda$ evolves similarly while $S$ increases. At $z = 3.5$, $\lambda$ remains at an almost constant level for $S \leqslant 0.27$ while for higher $S$ levels, $\lambda$ increases abruptly. For instance, an increase of 23 and 70% of the characteristic width with regard to the one obtained under static conditions is observed for $S$ equal to 0.34 and 0.57,

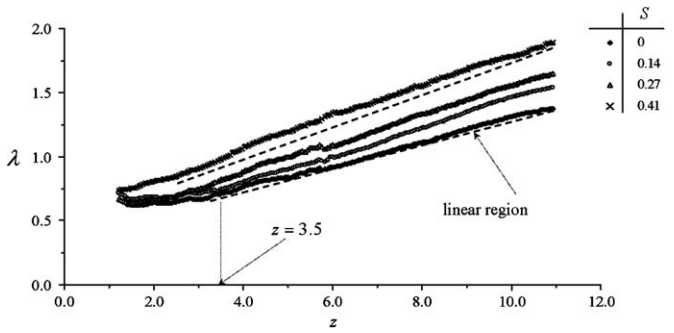


Fig. 4. $\lambda$ change with regard to $z$ for several $S$ levels.

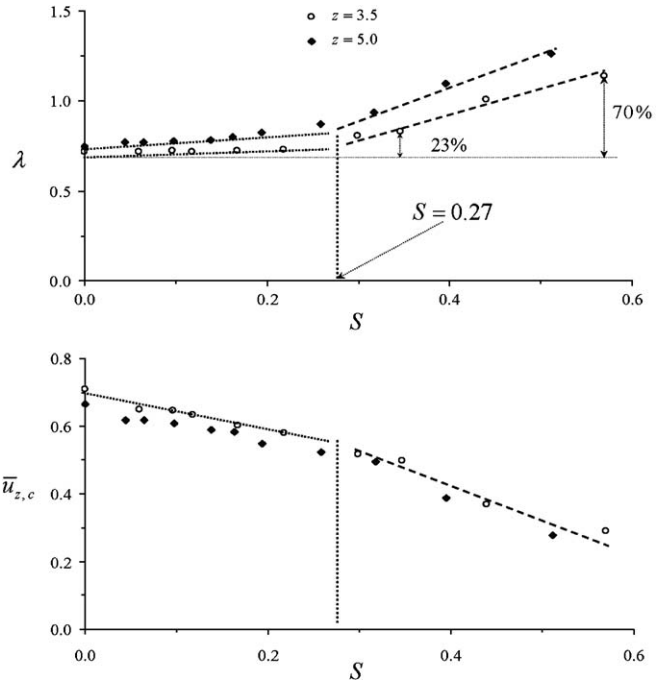


Fig. 5. Change of the radius of plume $\lambda$ and the center line mean axial velocity component $\bar{u}_{z,c}$ with regard to $S$.

respectively. The same trend occurs in the change of the centreline velocity magnitude with regard to $S$; as soon as swirling conditions are applied, $\bar{u}_z$ decreases slightly and such a decrease is amplified for $S \geqslant 0.27$. A threshold frequency ($S = 0.27$) is then clearly emphasized. Above such a level, i.e., for $S > 0.27$, the ascendant flow appears to be modified under swirling conditions while on the contrary, below the critical swirling number $S$ (i.e., $S \leqslant 0.27$), the main features of a static plume are conserved. As already stated by Elsner and Kurzak (1989) in the case of non-isothermal swirling jets, rotation induces sheared flows which, through viscosity forces, enhance lateral development and as a consequence reduce main component velocity magnitude. However, in natural convection flows such as pure thermal plumes, forces driving the ascendant flow are related to buoyancy and the latter is as high as the temperature gradients in the flow. It should be added that change of temperature under rotating conditions may greatly affect velocity amplitude of the flow field. To better describe flow field behaviour, analysis of the decay of $\bar{u}_{z,c}$ and $\overline{\Theta}$ with regard to $z$ has been performed.

Fig. 6 shows the change of the non-dimensional vertical velocity component and temperature with regard to $z$ under swirling conditions. In the non-swirling case, the modifications of the normalised velocity and temperature with $z$ underscore power laws in the fully turbulent region of the plume. These laws were put forward from static conditions. For $z > 4.0$, $\bar{u}_{z,c}$ and $\overline{\Theta}_c$ follow a $-1/3$ and $-5/3$ power law, respectively. In addition, observation of these laws clearly indicates the turbulent behaviour of the thermal plume as stated in analytical descriptions (Shabbir and George, 1994; Dehmani et al., 1996a). As soon as

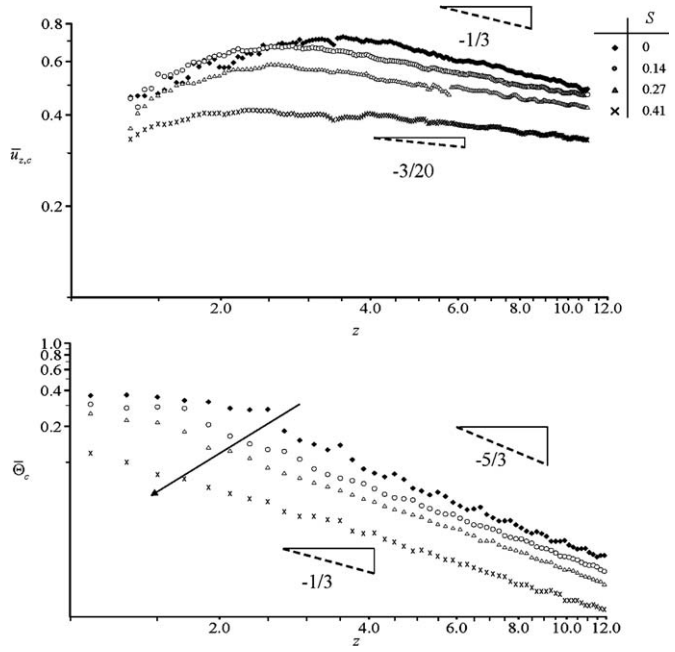


Fig. 6. Change of the normalized $\bar{u}_{z,c}$ mean axial velocity component and the normalized $\bar{\Theta}_c$ mean temperature along the geometrical axis function of $S$.

source swirling conditions are applied, the ascendant motion is affected; velocity magnitudes are lower while increasing $S$ and the change of $\bar{u}_{z,c}$ with regard to $z$ is altered. Even though the power law is not pronouncedly modified under swirling conditions, its power coefficient does decrease. For instance, for $S = 0.41$, the decrease of velocity with regard to $z$ is much smaller with a coefficient equal to $-3/20$ than the decrease observed in the static case. It is likewise true that the power law is followed over a wider range of $z$ under swirling conditions, as though rotation favoured the transition mechanism from laminar to turbulent regime. The same trend may be pointed out while studying the decrease of temperature along the geometric axis of the plume under rotating conditions as the power law coefficient varies from $-5/3$ to $-1/3$ from static case to $S = 0.41$. Let us now describe how lateral flow field behaves.

Lateral flow field expansion is highlighted by following the non-dimensional axial velocity component with regard to $r/\lambda$ at several heights (Fig. 7). Gaussian distribution perfectly fits the experimental data in the static case and as long as the swirling motion remains below the critical swirling number ($S \leqslant 0.27$), Gaussian distribution is still valid in depiction of flow field behaviour. However, the velocity

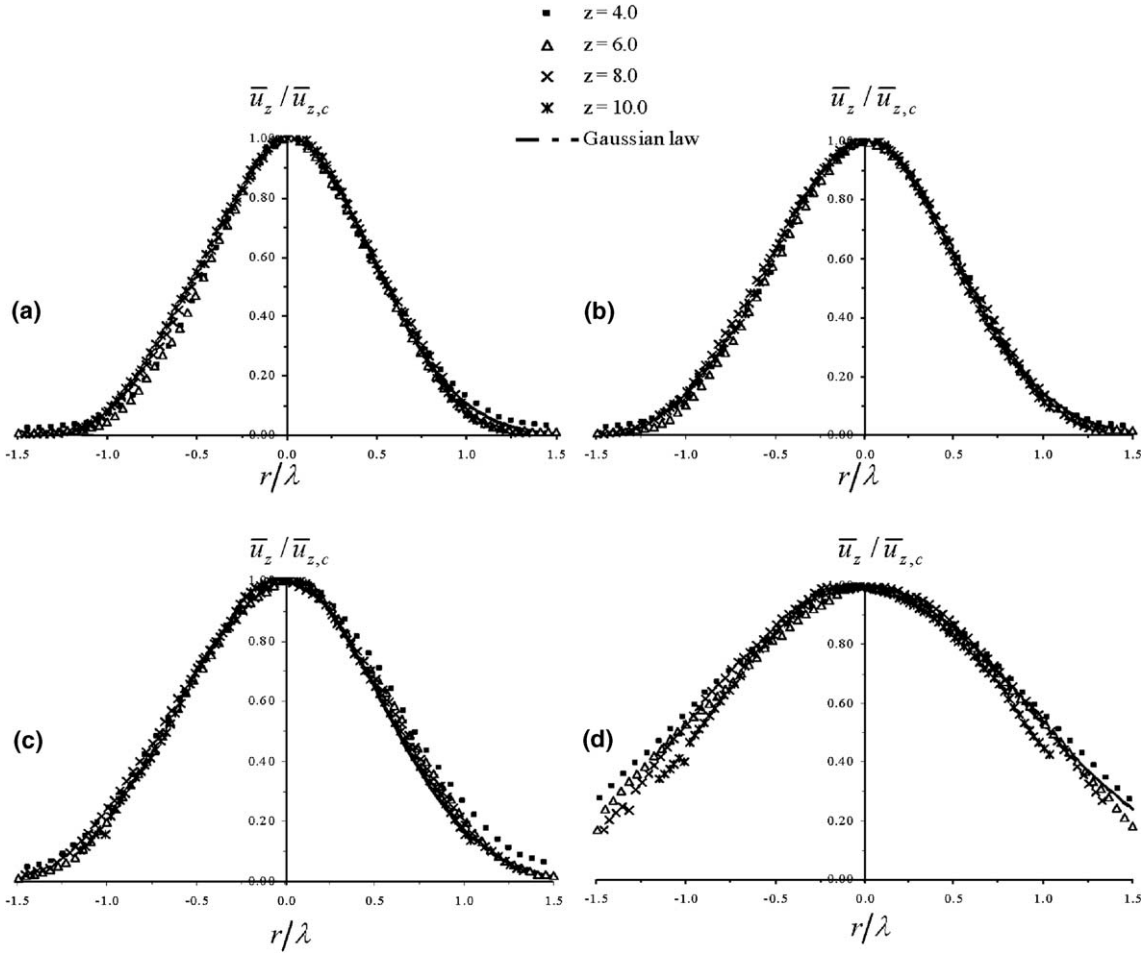


Fig. 7. Normalized radial profiles of the $\bar{u}_z$ mean axial velocity component with regard to $S$: (a) $S = 0$, (b) $S = 0.14$, (c) $S = 0.27$ and (d) $S = 0.41$.

profiles obtained at the highest swirling frequency ($S = 0.41$) reveal some changes from one profile to another, thereby showing that instability may arise in flow development. Results clearly demonstrate that above the threshold swirling number, most of the laws depicting pure thermal plumes remain valid, even if some coefficients are modified, whereas for $S$ levels higher than the critical value, the flow under such rotating conditions is affected. To better understand flow field behaviour under swirling conditions, it is essential to stress that flow is driven by two opposed forces. The first, which is the dominant one, is buoyancy force, while the second is linked to motion imposed by the disk rotation. In order to analyse the influence of source rotation, let us simply consider the case of a swirling non-heated disk. When a fluid layer, adjacent to the disk rotates along with it and slightly away from the source, the effect of centrifugal force creates a radial outward flow (Von Karman, 1921). Thus, radial and vertical motions due to the rotating disk are opposite to those which develop from a pure static plume. The effects of rotation are generally assumed to be confined close to the source location, and it is possible to advance the hypothesis that one effect of centrifugal force is to reduce the amount of entrainment into the plume. However, such an assumption in no way takes into account interaction between buoyancy and centrifugal forces, and it particularly ignores how turbulent activity develops when the two mechanisms arise simultaneously. The next section shall focus on the way swirling motion interacts from a turbulent point of view.

### 3.2. Turbulent characteristics

According to classical analysis dedicated to pure thermal plume behaviour (Nakagome and Hirata, 1976; Beuther and George, 1982) turbulent characteristics are often studied by following them along the geometrical axis of the plume. Actually, such parameters enable one to locate transition mechanisms from laminar to turbulence, which helps to explain why many researchers have focused on the change of normalized temperature and velocity fluctuations along the plume axis; as stated by Nakagome and Hirata (1976) and Georges et al. (1977), just to quote a few, behaviour of fluctuation intensities converges towards a constant level as soon as a fully turbulent regime is reached. As it is classically observed in experimental results, maxima of turbulent activity are reached before an asymptotic trend towards a constant level occurs. This behaviour is clearly observed in the change of thermal turbulent activities with regard to $z$ in the non-swirling case (Fig. 8(a)); first of all, $I_{t,c}$ decreases with regard to $z$ at levels lower than 10% for $z \sim 1.8$ before reaching a maximum equal to ≈40%. Then, the asymptotic change described above arises and a constant level of 35% is reached for $z \geqslant 4.0$. Swirl of the disk directly alters turbulent profiles; the location of maxima of thermal turbulent intensity occurs at an altitude lower than the one observed in the static case and its magnitude is amplified. At $S = 0.14$ for

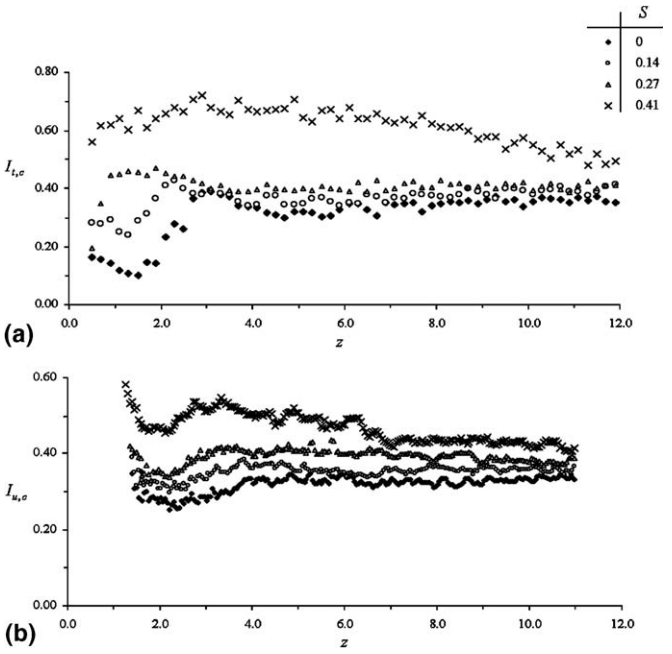


Fig. 8. Mean turbulent intensity distribution along the geometrical axis with regard to $S$: (a) $I_{t,c}$ thermal turbulent intensity and (b) $I_{u,c}$ dynamic turbulent intensity.

instance, $I_{t,c}$ the maximum level reaches 40% at $z \sim 2.2$ while at $S = 0.27$ the maximum arises at $z = 1.2$ at a level close to 44%. For levels above the swirling number threshold (at $S = 0.41$), $I_{t,c}$ are strongly affected with values higher than 60% and even up to 70% at $z = 3.5$. In addition, the constant level towards which $I_{t,c}$ converges is linked to the magnitude of the disk rotation; the higher the frequency, i.e., the higher the swirling number $S$, the higher the constant level of the thermal turbulent activity level. This trend is similarly observed when following fluctuating velocity intensity $I_{u,c}$ with regard to $S$ (Fig. 8(b)). As stated by Georges et al. (1977), similar behaviour occurs between thermal and dynamic fluctuations which are actually confirmed in the data shown in Fig. 8(b). A constant level of $I_{u,c}$ is reached at a given $z$ but contradictorily to thermal turbulent intensity, $I_{u,c}$ firstly decreases with $z$, reaches a minimum level and then asymptotically converges towards a constant level. As already observed in the thermal field, swirl condition greatly affects the magnitude of $I_{u,c}$. For instance, the level of $I_{u,c}$ reached is equal to approximately 34%, 36%, 40% and 46% for $S = 0$, 0.14, 0.27 and 0.41, respectively. The turbulent data clearly underline that turbulent levels are globally increased under swirling conditions. It is important to emphasize that due to rotation, loss of momentum may directly affect the ratio corresponding to $I_{u,c}$ levels. Table 2 gives the main characteristic fluctuating levels which suggest, contrarily to the thermal and dynamic turbulent intensity levels, that the dimensional turbulent levels either remain at a constant level or slightly decrease with the increase of the swirling frequency of the disk; amplification in the turbulent inten-

Table 2
Mean and second order moments of the vertical velocity components at $z = 5.0$

| $S$ | 0.0 | 0.14 | 0.27 | 0.41 |
|---|---|---|---|---|
| $\sqrt{\overline{u_{r,c}'^2}}$ | 0.110 | 0.109 | 0.105 | 0.104 |
| $\sqrt{\overline{u_{\theta,c}'^2}}$ | 0.111 | 0.108 | 0.106 | 0.105 |
| $\sqrt{\overline{u_{z,c}'^2}}$ | 0.149 | 0.137 | 0.136 | 0.131 |
| $\bar{u}_{z,c}$ | 0.654 | 0.578 | 0.505 | 0.384 |

sity is then mainly due to momentum decrease linked to swirl motion.

To precisely pinpoint where transition between laminar and turbulence occurs is a very difficult task and perhaps remains only a highly theoretical point of view. In most of the works found in the literature, the transition location may vary from one study to another. Such variations are either due to experimental set-up by itself or due to experimental difficulties hindering precise determination of flow field in this specific region. However, to be able to compare transition location from one work to another, researchers often refer to the transition location where maximum turbulent intensity occurs. From results shown in Fig. 8, it is possible to locate the fully turbulent region with regard to $S$. While under static conditions a maximum of thermal turbulent intensity is reached at $z = 3.5$, such a maximum peak is obtained at $z \sim 2.3$ and 1.5 for $S$ equal to 0.14 and 0.27, respectively. Note that for the highest $S$ studied ($= 0.41$), no maximum peak is observed any longer but that high turbulent levels are already reached in the vicinity of the heated disk. Thus, swirling conditions promote transition from laminar to turbulence and the higher the swirling number $S$, the sooner the transition occurs. Unstable mechanisms are then amplified resulting in fully turbulent flow but we still need to know whether or not entrainment mechanisms are likewise amplified.

### 3.3. Entrainment mechanisms

Entrainment of jets and plumes is of major interest and most of the authors of works dedicated to such flows have tried to better understand and describe entrainment phenomena. The entrainment concept, which is still valid today, was first introduced by Morton et al. (1956) and Turner (1969). This concept mainly states that a turbulent buoyant element expands at the expense of the quiescent surrounding fluid through entrainment of exterior fluid. It has indeed been established that entrainment velocity $v_e$ is directly proportional to vertical velocity and that such a proportionality coefficient $\alpha$ is a constant. As a result, experimental works have mainly focused on estimating the entrainment coefficient. The entrainment coefficient has been found to be constant even if its magnitude changes from one experimental set-up to another. Such changes may be linked either by the experiment itself or the way of measuring $\alpha$. Classical values of $\alpha$ entrainment coefficient found in the literature are referred to average data as first the entrained mass flow rate is estimated:

$$\dot{m}_e = \Delta\dot{m} = \dot{m}_2 - \dot{m}_1 \quad \text{with } \dot{m} = \int_0^\infty \rho u_z 2\pi r \mathrm{d}r$$

Then $\alpha$ is computed as

$$\alpha = \frac{\dot{m}_e}{\Delta z} \frac{1}{2\pi\rho_\infty \lambda \bar{u}_{z,c}}$$

Even though this definition has been used up until now by most researchers, two major drawbacks may be pointed out. First, when estimating the mass flow rate in a plume section or when using average velocity, the fluid density variation across the plume section needs to be taken into account and the $\overline{\rho' u'}$ fluctuating part also contributes to the entrainment. Let us advance the hypothesis that to precisely determine the contribution of the fluctuating term is a complex task insofar as it requires simultaneous measurement of fluid density (temperature) and velocity. Dibble et al. (1987) estimated that the contribution of $\overline{\rho' u'}$ fluctuating part corresponds to a 20% increase in mass flow rate. Second and surely by far the most restrictive assumption, $\alpha$ is always characterised by average quantities so that it is not possible to describe in time the change of the entrainment coefficient. However, it is classically admitted that in plumes or jets, coherent structures literally drive flow field development. And so, it would not be surprising that entrainment features were altered with regard to time by coherent structure convection. To be able to estimate change of $\alpha$ in time as accurately as possible, it is necessary to assess a coefficient entrainment in a way different from those that have been employed up to now. Actually, we have successfully developed a direct measurement technique on a static pure thermal plume enabling one to assess to time-dependent analysis of the entrainment mechanisms (Pham et al., 2005). In order to briefly sum up the principle of our technique which was applied for the first time to pure thermal plume, one needs to remember the basic idea established in the sixties by Ricou and Spalding (1961) who tried to measure entrained mass flow rate by co-axially surrounding a jet with a porous plate. According to them, pressure loss through the porous medium corresponds directly to a precise amount of mass flow rate attracted by the vertical motion. However, such an experimental set-up provides significant errors and cannot guarantee the flow field integrity to study. However, it remains true that measuring flow field outside the plume section is definitely an interesting way of investigation. When doing so, entrainment measurements are not altered by density fluctuations which exist inside the plume because as long as plume evolves in a constant and known environment, no fluctuation of density arises in the momentum term. To directly measure entrained mass flow rate, the PIV measurements described in Section 2 are necessary and direct mass flow rate entrainment is defined as

$$\dot{m}_e = \rho_\infty \int_{z_1}^{z_2} u_n 2\pi r \frac{dz}{\cos\beta}$$

by integrating velocity along a boundary surrounding the plume section at a vertical location at which $\alpha$ is required. However even if the surface which limits the main ascendant flow field is not as easy to define, a conical surface with a $\beta$ tilted angle with regard to the $z$ vertical direction has been found to be a good choice for the surrounding surface. $\beta$ is chosen as the angle at which plume expands laterally in average, i.e., it explicitly means that border of the plume is defined at $\lambda(z)$. Analysis of the accuracy of such a method has been performed. Influence of $\beta$ in the entrainment data may be considered as negligible (Pham et al., 2005). Actually, due to mass conservation, the $r.\ u_r$ term remains at a constant level. Then, the key point to address is to accurately measure the lateral flow field velocity which corresponds to very small levels in comparison with vertical velocity magnitudes. Such accurate measurements with PIV technique are possible insofar as the time delays between two images to correlate are adapted to the velocity amplitude to measure. To ensure accuracy of the direct method, location of the surface integration was shifted by 20% and such a change provides less than 2% difference in the $\dot{m}_e$ estimation. Such a result confirms how accurate the direct method is and the latter has been employed under swirling conditions to help us to more clearly depict the influence of source rotation on the entrainment process.

Then, direct measurement method allows one to evaluate $\alpha$ change in time by integrating instantaneous velocity distribution. Fig. 9 presents such change with regard to the swirling number $S$ level for two different $z$ vertical locations ($z = 3.0$ and $z = 5.0$). As far as we know, this is the first time that $\alpha$ entrainment coefficient has been followed in time and that $\alpha$ presents some significant variations which fluctuate here and there from an average value. At $z = 3.0$ under static conditions, fluctuations of $\alpha$ are smoother than those observed for higher swirling number $S$ because at that location, turbulent flow field has yet to be established. Abrupt changes in time are amplified under swirling conditions. In addition, such sudden variations are amplified at $z = 5.0$. This explicitly means that mechanisms exist which either favour or prevent entrainment. Fig. 10 presents instantaneous velocity distribution in a $x$–$y$ plan at two different times; Fig. 10(a) corresponds to $t = 1.8$ s when $\alpha$ reaches its maximum level under static conditions while Fig. 10(b) presents velocity vectors at a time when on the contrary the main flow pattern patterns are inward-oriented. Such behaviour underscores one entrainment feature of the flow at that time. Following $\alpha$ variation with regard to $S$, it is obvious that the higher the swirling frequency, the stronger the fluctuating levels of $\alpha$. In addition, $\alpha$ average levels are also linked to the rotation frequency imposed at the heated source. To underline this trend Table 3 lists the average and fluctuating levels of $\alpha$

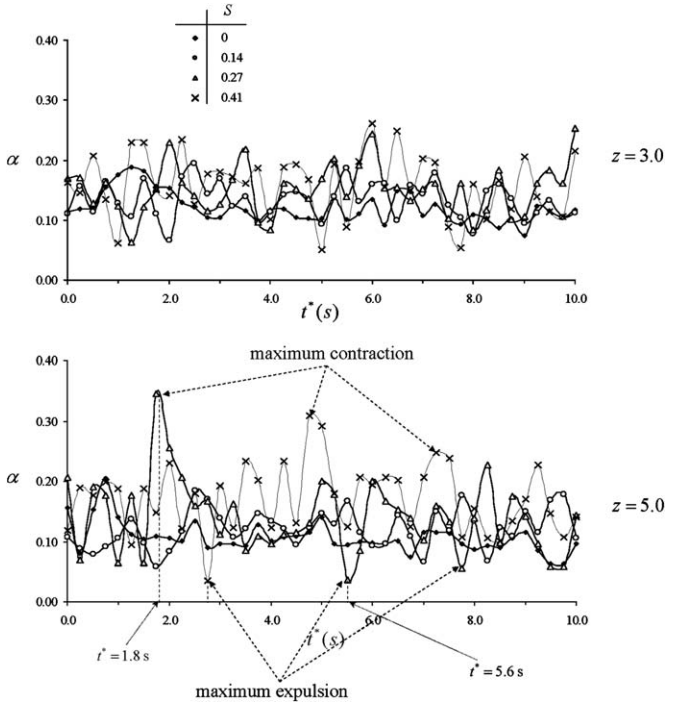


Fig. 9. Instantaneous entrainment coefficient $\alpha$ with regard to $S$ at $z = 3.0$ and $z = 5.0$.

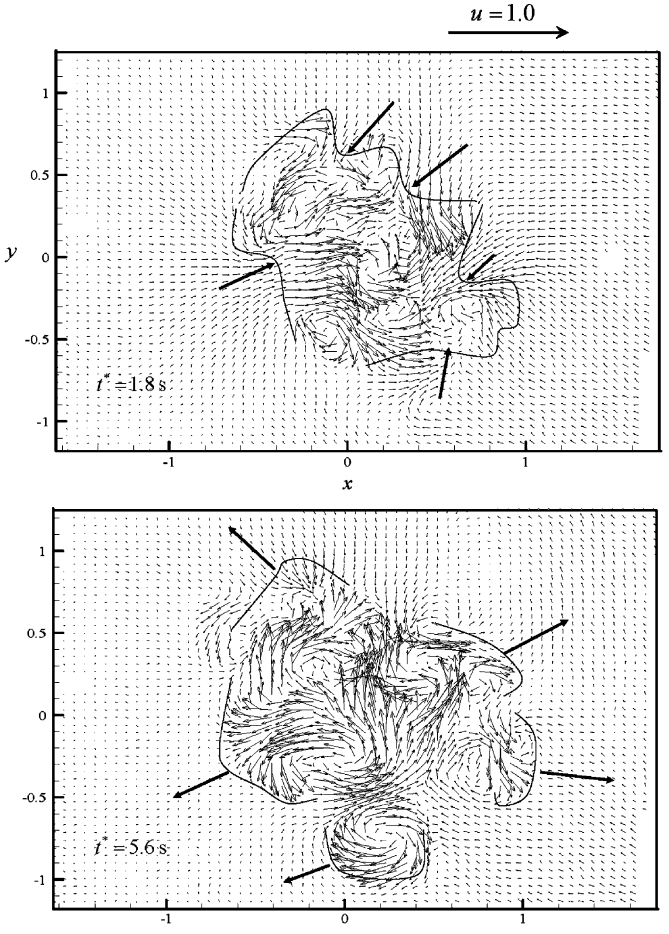


Fig. 10. Instantaneous velocity field in a $x$–$y$ plane at $z = 5.0$ plane for two $t^* = 1.8$ s and $t^* = 5.6$ s under swirling condition $S = 0.27$.

Table 3
$\bar{\alpha}$ and $\sqrt{\overline{\alpha'^2}}$ levels of entrainment coefficient $\alpha$ with regard to $S$ at $z = 3.0$ and $z = 5.0$

| $S$ | $z = 3.0$ | | $z = 5.0$ | |
|---|---|---|---|---|
| | $\bar{\alpha}$ | $\sqrt{\overline{\alpha'^2}}$ (%) | $\bar{\alpha}$ | $\sqrt{\overline{\alpha'^2}}$ (%) |
| 0.0 | 0.115 | 18.0 | 0.107 | 20.0 |
| 0.14 | 0.122 | 22.0 | 0.115 | 25.0 |
| 0.27 | 0.144 | 24.5 | 0.133 | 30.2 |
| 0.41 | 0.179 | 29.5 | 0.176 | 36.5 |

with regard to $S$ for the two vertical locations shown in Fig. 9. One may readily notice that under strong swirling conditions, i.e. for the highest $S$ shown (0.27 and 0.41), the contraction as well as the expulsion phases are amplified; for instance, at $z = 5.0$, the expulsion phases are so significant that from time to time entrainment is almost prevented. To our knowledge, Basu and Narasimha (1999) were the first to put forward the development of large expulsive motions at certain transverse cross-sections while studying numerically turbulent flows with cloud-like off-source heating. One may also note that Julien et al. (1999) analysed plume development in rotating conditions but were in fact considering the overall exterior fluid under rotating conditions; they put forward the hypothesis that expansion of the turbulent plume by entrainment of exterior fluid may be suppressed by strong rotation under such conditions. When the heated source rotates, such motions are clearly observed experimentally. Experimental data and their variations with time highlight the existence of two different phases, one favouring entrainment during contraction with the other trying to suppress entrainment from time to time. Swirling of a heated source amplifies the intensity of those two opposite phases but net mass flow rate balance always remains positive, i.e. even if strong fluctuations occur in the change of $\alpha$ with time, the average level of $\bar{\alpha}$ is still significant and as observed in Table 3, the latter has a tendency to increase along with the increase of $S$. In order to emphasise $\bar{\alpha}$ changes with time, its probability density function was computed with regard to $S$ at $z = 5.0$, i.e., in the fully turbulent region (Fig. 11). At that height and under static conditions, pdf distribution is relatively centred on its mean level equal to 0.11 approximately. However, pdf distribution is directly affected by the source rotation. Insofar as $S$ is increased, i.e., the rotation frequency is amplified, pdf distribution becomes broader and broader. For instance at $S = 0.14$, even if distribution still remains centred around its average value, $\alpha$ presents stronger variations on both sides of its average value and the process is amplified for $S = 0.27$ and 0.41. Under the swirling conditions we have just indicated, significant values of $\alpha$ are spread over a large range of values extending from almost $\alpha = 0.0$ up to 0.28. To quantitatively underline how much pdf distribution enlarges, one may put forward the hypothesis that its characteristic width is up to 3 times larger for $S = 0.41$ than under static conditions. Actually, it is essential to point out that under static conditions, larger $\alpha$ pdf distribution is also obtained but that its change with regard to $z$ is much lower than under swirling conditions; this clearly indicates that rotation of the source generates shear-layer development interacting directly with the coherent structures. It actually favours breakdown of coherent structures and rotation effect may be seen as a speeding process within the structure alteration.

Lastly, Fig. 12 presents profiles of the average value of $\bar{\alpha}$ along the $z$ vertical direction for different swirling

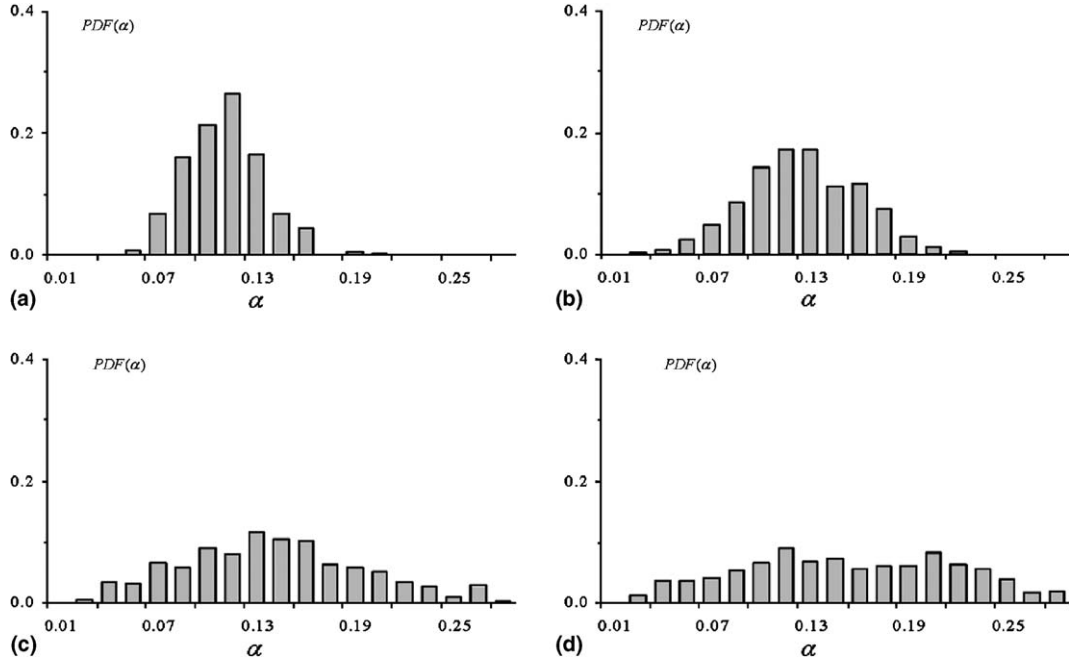


Fig. 11. Probability density function of entrainment coefficient $\alpha$ with regard to $S$ at $z = 5.0$. (a) $S = 0$, (b) $S = 0.14$, (c) $S = 0.27$ and (d) $S = 0.41$.

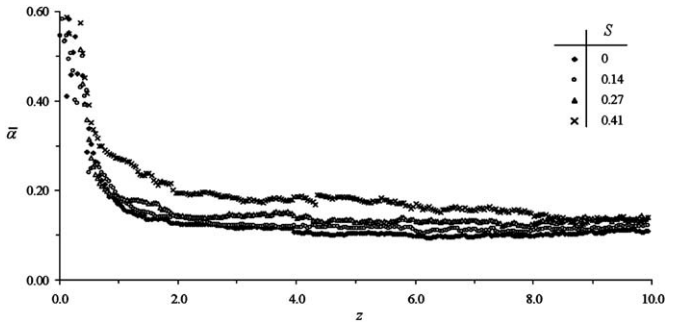


Fig. 12. Variation of mean entrainment coefficient $\bar{\alpha}$ along vertical axis $z$ with regard to $S$.

conditions. Under static conditions ($S = 0$), $\bar{\alpha}$ is measured all along the plume development and even in the vicinity of the heated source. In this region $\bar{\alpha}$ reaches very high levels with maxima close to 0.6 before it decreases towards constant and much smaller levels in the turbulent region. In fact, the levels reached in the vicinity of the heated source are nearly 6 times higher than its constant level in the turbulent region. It is true that due to buoyancy force which develops close to a heated source, attraction of exterior fluid is highly significant and entrainment is so strong in this area that the vertical flow section is reduced up to a minimum level. Under swirling conditions, profiles of $\bar{\alpha}$ with $z$ are similar to the one obtained under static conditions. Note that data obtained in the vicinity of the heated source are similar whatever the $S$ levels. However, in the fully turbulent region the magnitude of the $\bar{\alpha}$ coefficient is different. As already observed through results listed in Table 2, swirling motion favours entrainment, i.e., as soon as the heated source rotates, it amplifies the entrainment capacity of the vertical flow.

## 4. Conclusion

Present experimental results are dedicated to pure thermal plume behaviour while its heated source is under swirling conditions. To fully interpret such influence, results from a static case were compared with those obtained under several swirling frequencies. Shear is amplified close to the source under swirling conditions and its consequences are double: the transition location is directly influenced by the swirling motion and the higher the frequency the smaller vertical location at which transition occurs. In addition, levels of dynamic and thermal turbulent intensities are amplified along with the increase of the swirling frequency, i.e., along with the increase of the swirling number. A threshold swirling number has been put forward. Under such a threshold level, i.e., under low frequency rotation, flow behaves like a pure thermal plume in such a way that most of the classical laws describing a pure thermal plume may still be applied. However, for a high swirling number, coefficients of such well-known laws, such as for instance the decrease of axial velocity and temperature, are modified even if similar behaviours are still exhibited.

Three-dimensional and instantaneous measurements allow one to shed light on the role of vortex structures on entrainment mechanisms. Two major phases, the expulsion and contraction phases, drive the entrainment mechanisms under strong swirling conditions, i.e., at a high swirling number, these two phases are amplified to such an extent that entrainment is from time to time either inhibited or amplified by a ratio of 3, yet the net balance between expulsion and contraction always remains positive, i.e., the ascendant motion still retains its entrainment capability. Such a point differs fundamentally from findings dedicated to plumes evolving in a rotating environment; this discrepancy constitutes a major issue to be addressed in the near future. It would also be interesting, in cases similar to the one detailed in the present study, that unstable growth between gravity and centrifugal forces be fully described. Due to the difficulties facing experimenters attempting to fully depict flow in the vicinity of the heated source, direct numerical simulations may be of great help when assessing driving instability development.

## References

Agator, J.M., Doan Kim, S., 1982. Turbulent structure of axisymmetric thermal plumes. Mech. Res. Commun. 9, 159–162.

Agrawal, A., Prasad, A.K., 2004. Evolution of a turbulent jet subjected to volumetric heating. J. Fluid Mech. 511, 95–123.

Alkislar, M.B., Lourenco, L.M., Krothapalli, A., 2000. Stereoscopic PIV measurements of screeching supersonic jet. J. Visual. 3, 135–143.

Ayotte, B.A., Fernando, H.J.S., 1994. The motion of a turbulent thermal in the presence of background rotation. J. Atmos. Sci. 51, 1989–1994.

Bastiaans, R.J.M., Rindt, C.C.M., Nieuwstadt, F.T.M., Van Steenhoven, A.A., 2000. Direct and large-Eddy simulation of the transition of two- and three-dimensional plane plumes in a confined enclose. Int. J. Heat Mass Transfer 43, 2375–2393.

Basu, A.J., Narasimha, R., 1999. Direct numerical simulation of turbulent flows with cloud-like off heating. J. Fluid Mech. 385, 199–228.

Beuther, P.D., George, W.K., 1982. The turbulent plume in a stratified environment. in: Proc. Natl Congr. Theor. and Appl. Mech.. Cornell University, Ithaca (NY).

Bill, R.G., Gebhart, H.D., 1975. The transition of plane plumes. Int. J. Heat Mass Transfer 18, 513–526.

Dehmani, L., Doan Kim, S., Ghaboue, L., 1996a. Turbulent structure of an axisymmetric plume penetrating a strong density stratification. Int. J. Heat Fluid Flow 17, 452–459.

Dehmani, L., Doan Kim, S., Gbahoue, L., Rongère, F.X., 1996b. Influence of a strong density stratification axisymmetric plume. Exp. Fluids 21, 170–180.

Dibble, R.W., Schefer, R.W., Chen, J.Y., Hartmann, V., 1987. Velocity and density measurements in a turbulent nonpremixed flame with comparison to numerical model predictions. Sandia Report, SAND85-8233, UC-304.

Elsner, J.W., Kurzak, L., 1989. Semi-preserving development of a slightly heated free swirling jet. S. Fluid Mech. 199, 237–255.

Georges, W.K., Alpert, R.L., Taminini, F., 1977. Turbulence measurements in an axisymmetric buoyant plume. Int. J. Heat Mass Transfer 20, 1145–1154.

Guillou, B., Doan Kim, S., 1983. Etude theorique du développement d'un panache thermique a symétrie axiale – influence des propriétés thermophysiques du fluide. Int. Commun. Heat Mass Transfer 10, 101–109.

Helfrich, K.R., 1994. Thermals with background rotation and stratification. J. Fluid Mech. 259, 265–280.

Julien, K., Leff, S., McWilliams, J., Werne, J., 1999. Plumes in rotating convection. Part 1 Ensemble statistics and dynamical balances. J. Fluid Mech. 391, 151–187.

Morton, B.R., Taylor, G., Turner, J.S., 1956. Turbulent gravitational convection from maintained and instantaneous sources. P. Roy. Soc. Lond. 234 A, 1–24.

Muñiz, L., 2000. Particle image velocimetry studies of turbulent non-premixed flames, Ph.D. thesis. Stanford University, Stanford, CA.

Nakagome, H., Hirata, K., 1976. The structure of turbulent diffusion in an axi-symmetrical thermal plume. In: Proc. of the ICHMT Conf. on Turbulent Buoyant Convection 9, 361–372.

Pham, M.V., Plourde, F., Doan Kim, S., 2005. Three-dimensional characterization of a pure thermal plume. J. Heat Transfer 127, 1–13.

Ricou, F.P., Spalding, D.B., 1961. Measurements of entrainment by axisymmetrical turbulent jets. J. Fluid Mech. 11, 21–32.

Shabbir, A., George, W.K., 1994. Experiments on round turbulent buoyant plume. J. Fluid Mech. 275, 1–32.

Taylor, G., 1945. Dynamics of a mass of hot gas rising in air. US Atomic Energy Commission, MDDC-919, LADC-276.

Turner, J.S., 1969. Buoyant plumes and thermals. Annu. Rev. Fluid Mech. 1, 29–44.

Von Karman, T., 1921. Uber Laminare und Turbulente Reibung. ZAMM 1, 233.